# BIAXIAL FATIGUE TESTS ON THIN WALLED TUBES OF NICR23CO12MO (INCONEL 617) AT 950 °C

H.-P. Meurer, H. Hanswillemenke, H. Breitling, W. Dietz

Interatom GmbH

5060 Bergisch Gladbach 1

West Germany

## ABSTRACT

For the design of components for the High Temperature Gas Cooled Reactor the failure criteria developped by uniaxial fatigue tests have to be verified for multiaxial fatigue loading. The paper describes the experience gained with the installation of a biaxial fatigue test facility and some results on thin walled tubes of NiCr23Co12Mo (Inconel 617) at 950 °C. Uniaxial and biaxial fatigue tests at strain ranges between 0.3 % and 1 % have been performed. The v. Mises equivalent strain hypothesis gave a good fit of the fatigue results. The deformation and hardening behaviour is described.

## I INTRODUCTION

Fatigue loading imposed by start up/shut down operations or power transients is a principal cause of failure in power plants. In general the fatigue loading in a component is of a complex multiaxial nature. There are different ways in treating multiaxial fatigue which depend e. g. on the actual material and the loading situation [1 - 3]. The mostly applied engineering method is to reduce the multiaxial straining to an

equivalent unaxial strain and then to perform the design analysis on the basis of unaxial fatigue data. For ductile materials which are applied as structural materials in power plants, the distortion energy hypothesis (von Mises) is used to reduce the multiaxial strain to an equivalent unaxial strain, see e. g. the ASME Code Case N47. For torsional and combined torsional-axial-in-phase loading this method gives good or at least conservative predictions whereas for combined out-of-phase-loading often unconservative results are reported. The development of the High Temperature Gas Cooled Reactor is aimed at temperatures up to 950 °C in the primary circuit and the heat exchanging components. The most promising alloy for these service temperatures appears to be the Ni-base alloy NiCr23Co12Mo (≙ Inconel 617) [4]. For this alloy neither multiaxial fatigue data nor design rules for applications up to 950 °C did exist which gave rise to the experiments reported here.

## II. EXPERIMENTAL

### II.1 LOAD FRAME, TEST CHAMBER AND SPECIMEN GEOMETRY

For multi-axial fatigue testing several different test configurations have been applied: single load systems with specimens of variable geometry to obtain different biaxial stress conditions and multiple load systems with fixed specimen geometries [5]. These systems include the tension-torsion, tension-pressure, tension-torsion-pressure loading of tubular specimens and the biaxial loading of cruciform specimens. The choice of an appropriate system for HTGR related experiments was determined by the following requirements: Simulation of the fatigue behaviour of thin walled tubes especially for heat exchanger components and hot gas ducts, test temperatures up to 1000 °C under controlled environmental conditions, and last not least exact strain controlled loading conditions. The loading should be biaxial with the option of a further extension to a triaxial state of strain. These requirements could be best fulfilled with tension-torsion tests of thin walled tubes during

which well defined plane strain conditions could be introduced in the specimens. Furthermore most of the biaxial fatigue experiments were performed with this type of test configuration which facilitated the acquisition of an appropriate test system. The fatigue test system consists of a computer controlled servohydraulic test unit with independent loading of the axial and torsional direction. A view on the load frame is given in Fig. 1. The maximum load capacities are ±250 kN in axial direction and ±2.3 kNm in torque, the maximum displacements are ±100 mm and ±50°.

For tests under controlled environmental conditions which are essential for the evaluation of the fatigue behaviour of metallic materials at very high temperatures, a test chamber has been attached to the load frame, see Fig. 1. The test chamber allows for tests in vacuum as well as under pressurized helium up to 40 bar. In the current programme the tests have been performed in helium with defined small amounts of impurities, the composition of which is given in table 1, at a pressure of 1.8 bar and a flow rate of 3 ltr/h. These conditions are comparable to the primary circuit conditions of an HTGR. The leak tight sealing of the actuator which represented one of the major problems of the test chamber is achieved by a double sealing ring system together with a high precision manufacturing of the sealing surfaces of the clamping device. Under combined loading a vacuum better than $8 \times 10^{-6}$ mbar is achieved which guarantees that the diffusion of oxygen into the chamber occurs at very low levels.

To enable testing at temperatures up to 1000 °C the test chamber consists of a double walled construction with an internal cooling system which keeps especially the sealing of the different feedthroughs below 100 °C. In Fig. 2 the specimen geometry applied for these tests is shown. The inner surface was carefully honed whereas the outer surface was grinded and subsequently polished which led to a roughness $r_a \leq 0.5$ µm and tolerances in the outer diameter of less than 10 µm. A concentric mounting of the specimens was achieved by bolts

which fit into the specimens at each end with a clearance of less than 2 μm. The specimens have been clamped from outside against these bolts by a circular spring system which guarantees an undistorted transmission of the axial and torsional forces as can be seen later from the hysteresis loops. The clamping of the specimens against the inner bolts additionally secured the sealing of the inner volume of the specimen. The bolts contained a boring which could be either connected to the pressure chamber to allow the helium gas to flow through the specimen and thus prevent the oxidation of the inner surface or could be connected to an outer pressure system to perform at a later time tests under a triaxial state of strain. In the current tests the inner volume of the specimen was connected to the pressure chamber, i. e. a helium stream of 1.8 bar pressure passed with 3 ltr/hr through the specimen. This provided equilibrium with the outer pressure and due to the low flow rate no significant cooling of the inner surface occured.

## II.2 SPECIMEN HEATING AND TEMPERATURE DISTRIBUTION

The choice of the heating system was influenced by the requirements to perform tests up to 1000 °C, not to interfere with the composition of the test atmosphere, not to heat up the pressure chamber beyond 100 °C, to allow for a homogeneous temperature profile on the gauge length of the specimen but also for a sharp gradient to the specimens' clamping devices and last not least to give access for a strain measurement device for temperatures up to 1000 °C. Under these circumstances the best solution apeared to be an induction heating system. Some minor problems occured with the feedthrough of the induction coil tubes which had to be heat resistant, non conductive, and ductile to guarantee leak tightness during the operation of the chamber. With the choice of a special polymer these problems could be overcome. Furthermore the intensive electric field generated with the induction heating required very careful and extended grounding of all metallic components of the pressure chamber and of the loading rig to reduce the

noise signals in the different measurement devices and even to avoid sparking between different components.
But the main problem appeared to be the temperature measurement and distribution on the tubular specimens. First, only shielded thermocouples could be used to minimize the noise induced by the induction heating. The noise was found to be reduced further when the shielded thermocouples were orientated perpendicular to the specimens surface in contrast to a parallel orientation. Only shielded thermocouples of 0.5 mm diameter, the smallest available diameter, could be applied because the more stable thermocouples of 1.0 mm diameter led to a significant heat conduction from the surface inducing a temperature drop of up to 50 °C, depending on the fixture on the surface. In addition the thin walled tubes did not allow for drilling holes in the specimen surfaces to attach the thermocouples effectively. From all possibilities of a reliable coupling which on the other hand must avoid crack initiation during the fatigue tests the fixture of the thermocouples by 50 µm thin foils which themselves have been spotwelded to the specimens guaranteed the best results. By this procedure the thermocouple was for more than five times the thermocouple's diameter in contact to the specimen surface. Nevertheless the sharp temperature gradient at the surface to the surrounding atmosphere and the thermal conductivity of the thermocouple led to an error of -20 °C. But because this error was reproducable by ±2 °C it was tolerated and taken into account during the tests.

A gauge length of 50 mm required at least a uniform axial temperature distribution over 70 mm. During the optimization of the induction coil geometry the limited available length and the attachment of the extensometer as well as the available power of the heating system had to be considered. The temperature distribution could be considerably improved when nearly rectangular tubes were applied for the induction coil instead of round tubes because rectangular tubes generate a more extended penetration of the field into the specimens as compared to round tubes. Besides the axial temperature

distribution the circumferential temperature distribution needs special attention for thin walled tubes because the circumferential heat flux is restricted due to the small wall thickness. This requires a very low ovality of the induction coil as well as an exactly concentric mounting of the induction coil in the test chamber because the circumferential temperature distribution appeared to be very sensitive to small deviations of the location of the induction coil. Figure 3 gives a drawing of the final configuration of the induction coil and the axial temperature distribution achieved hereby. For the temperature measurement on a calibration specimen 5 thermocouples have been mounted along 70 mm on the gauge length. They have been attached with small welded plates and in drilled holes which give good coupling to the surface. The specimen had been rotated by steps of 45° and during each step the axial gradient had been measured. With this procedure the circumferential temperature distribution could be determined, too. A maximum axial deviation of less than 8 °C and a maximum circumferential deviation of 9 °C were found whereas the highest overall temperature difference between two points was less than 15 °C. From the current experience it seems to be very difficult to achieve a better temperature distribution even though a deviation within the range of ±5 °C would be desirable.

## II.3 STRAIN MEASUREMENT

At the time when the test facility was ordered worldwide no high temperature multiaxial strain measurement device was available. After trials performed by the manufacturer of the test facility it became clear that the only possible solution could be a biaxial extensometer to be developped on the basis of available unaxial strain measurement systems. In Fig. 4 the extensometer and its fixture and attachment to the hot specimen is shown. The axial and torsional displacement of the specimen is transmitted by a single pair of quartz rods to a set of two resistance type strain gauges which are protected by a water cooled shield from the radiation heat of the specimens. The strain gauges are mounted in a way that axial and circum-

ferential displacements are measured independently from each other practically without any crosstalk. The calibration curves - examples of which are shown in Fig. 5 - show the excellent accuracy and resolution of the extensometer. Even for the smallest axial strain range of $\Delta\varepsilon_A$ = 0.24 % the accuracy is better than 0.4 % of the actual value or less than 0.25 % of the full range. During the axial displacement the torsional signal nearly keeps zero as indicated by the crosses at the centre line of the upper diagramme in Fig. 5. The same was found at higher axial strain ranges and torsional displacements. The calibration of the axial or torsional displacement with a superimposed constant second component did not show an influence on neither of the two signals. During the fatigue experiments the extensometer was mounted on a column of its own which was fixed to the machine bed and coupled to the pressure chamber only by a vacuum below. This construction avoids possible interference with vibrations of the pressure chamber which might be induced by the friction of the loading piston with the seals.

## II.4 MATERIAL

The tests have been performed on tubes of NiCr23Co12Mo, almost equal to Inconel 617 (Trademark of the Inco. Co.). It is a solid solution hardened Ni-base wrought alloy which is regarded to be the most suitable alloy for applications as heat exchanging components at very high temperatures. The tubes which had an original diameter of 34.0 x 3.0 mm have been supplied in two lots, the chemical composition and room temperature strength values of which are given in Table 2. They were fabricated by Mannesmann pilger mill rolling and finally anealed for 30 min at 1200 °C and water quenched. This treatment resulted in a grain size of ASTM 4 which was identical for both lots. The material falls well within the specification for NiCr23Co12Mo and even though not identical it is not much different from the heats on which the uniaxial tests on standard specimens have been performed.

## II.5 TEST PROGRAMME

The test programme consisted of four different sets of experiments: pure axial loading, pure torsional loading, combined axial/torsional in-phase loading and combined axial/torsional loading with 45° phase angle. All tests were performed displacement controlled with a triangle wave form. For the axial component strain ranges $\Delta\varepsilon_A$ = 0.3 - 1.0 % and a strain rate $\dot{\varepsilon} = 4 \cdot 10\text{-}s^{-1}$ have been employed. For the torsional component the shear strain was chosen in a way that the same equivalent strain range $\varepsilon_{MT}$ as the axial strain $\Delta\varepsilon_A$ resulted. During the combined axial/torsional tests the ratio of equivalent strain of the torsional component to the axial strain was $\Delta\varepsilon_{MT}/\Delta\varepsilon_A = 1$. For the calculation of the equivalent strain the distortion energy hypothesis of ASME Code Case N47 was applied:

$$\Delta\varepsilon_M = \sqrt{(\Delta\varepsilon_A)^2 + \tfrac{1}{3}\ (\Delta\gamma)^2}$$

which assumes a Poisson's ratio $\nu = 0.5$.

# III. RESULTS

## III.1 FATIGUE LIVES

The fatigue lives obtained under uniaxial loading with thin walled tubes fit very well within the scatterband obtained for two other heats of NiCr23Co12Mo at 950 °C, Fig. 6. Only one experiment on the thin walled tubes has to be excluded which is indicated by brackets in Fig. 6 and upon which will be commented later.

When the fatigue lives of the axial, torsional, and combined axial-torsional experiments are plotted as a funcion of the equivalent strain $\Delta\varepsilon_M$ a surprisignly good correlation is obtained. Only the experiment at $\Delta\varepsilon_A = \Delta\varepsilon_{MT}$ = 1.0 % and ø = 45° gives a significantly lower fatigue life than predicted by the von Mises equivalent strain hypothesis. Excluding this experi-

ment the von Mises equivalent strain hypothesis describes the fatigue lives for all strain ranges very well, even at low strain ranges where deformation has a significant elastic component. The von Mises equivalent strain as applied in Code Case N47 assumes a Poisson's ratio of $\nu = 0.5$ which is valid for entirely plastic deformation. An examination of Richter [7] on the physical properties of NiCr23Co12Mo up to very high temperatures suggests $\nu = 0.35$ for elastic deformation. But this value has been determined dynamically. An evaluation of Young's and shear moduli of the first loading cycle of each experiment revealed a mean value $\nu = 0.5$ which justifies the assumption of Code Case N47 in the case of the behaviour of NiCr23Co12Mo at 950 °C.

One experiment with $\Delta\varepsilon_A$ which gave only 1/5 of the mean fatigue life was excluded from the evaluation. During the experiment the pressure within the tube was not kept at 1.8 bar but at normal pressure due to a malfunction of the throttle valve. Therefore, the helium flux increased which must have decreased the temperature of the inner wall considerably, thereby inducing a sharp temperature gradient over the specimen wall.

Some examples of failed specimens are given in Fig. 8. Under pure axial loading the crack is orientated circumferentially. Under pure torsional loading the cracks appear at two planes at angles of 45° with respect to the specimen's axis and are connected by one or more perpendicular cracks. Under in-phase loading the cracks are orientated at 45° with respect to the axis. For 45° out-of-phase loading two circumferential cracks connected by a vertical crack are observed at low strain ranges. At the highest strain range the specimen failed clearly by buckling and not by fatigue crack formation.

During all tests with a constant principal loading direction which are the test with pure axial, pure torsional, and in-phase loading, the crack is orientated normal to the principal loading direction. The torsionally loaded specimens contain only a small amount of tensile cracking (stage II cracking). In that way the cracking behaviour differs from that of austeni-

tic stainless steels at room temperature [8]. During 45° out-of-phase loading the cracks normal to axial and shear loading appear to have been formed relatively separately from each other.

## III.2 DEFORMATION BEHAVIOUR

Under continuous cycling at 950 °C the alloy NiCr23Co12Mo shows no cyclic hardening anymore [6]. This was intensively studied for uniaxial fatigue tests but the same features are observed in multiaxial tests. In Fig. 9 the cyclic hardening of different loading combinations is shown for $\Delta\varepsilon_A = \Delta\varepsilon_{MT} = 0.6$ %. The y-axis is given in normalized values of force and torque, the conversion factors $C_a$ to axial and $C_t$ to shear stresses - which are to be applied to the full range of the y-axis - are given, too. Both the axial and the shear stress remain constant for more than 90 % of the fatigue life, which indicates that the crack propagation phase in thin walled tubes is restricted to a short period. During uniaxial tests on solid specimens the crack propagation phase extends to over appr. 30 % of fatigue life due to the larger thickness of the specimens. The nearly constant stress behaviour also indicates that the specimens keep relatively stable until the start of the crack initiation phase. During the axial loading a negative mean stress developped already in the first cycle. The shear stresses always remained symmetrical without mean stress. The negative mean stress probably developped by the internal pressure of the test chamber which acted on the large clamping devices. During combined axial-torsional loading with a 45° phase angle a continuous decrease in the axial and shear stresses is observed from the very beginning of the test. The effect is even more pronouced at $\Delta\varepsilon_A = \Delta\varepsilon_{MT} = 1.0$ %. Because the cyclic hardening behaviour is not very likely to change significantly when a phase angle is introduced in combined loading it appears to be more likely that the stiffness of the specimen is decreasing. This was confirmed by the buckling observed for the failed specimen. Additional information on the deformation behaviour can be obtained from the hysteresis

loops as shown in Fig. 10a - d for strains $\Delta\varepsilon_A = \Delta\varepsilon_{MT} = 0.6$ %. The axis are once again normalized in strain and stress conversion factors are indicated. At 950 °C the alloy NiCr23Co12Mo can be plastically deformed without any strain hardening which is examined and discussed in more detail in ref. [6]. The behaviour under axial or torsional loading is not much different, s. Fig. 10a + b. Even under combined loading no drastic changes occur, Fig. 10c. But both the axial and the shear stresses are reduced compared to pure axial or torsional loading. The reduced maximum stresses can easily be explained by Mohr's circle. Putting axial and shear stress together in Mohr's circle a uniaxial stress of 210 MPa would result which is close to the experimental value of 190 - 200 MPa.
During the biaxial fatigue experiments at 45° phase angle the hysteresis loops are significantly distorted. For a better demonstration of the yielding behaviour the points of identical loading times are indicated. The shear stresses increase rapidly when the axial stresses have changed the loading directions, points 1 and 3 in Fig. 10d. The maximum shear stress is achieved when the axial stress is zero and at that point it is equal to the shear stress measured in pure torsion. The axial stress reacts in a similar way on the out-of-phase loading of the shear stress. An evaluation shows that the resulting flow stresses do not deviate significantly from Mohr's circle.

## V Summary

The installation of a biaxial tension/torsion fatigue test facility with an option for triaxial loading has been described. A pressure chamber allows for tests under vacuum of better than $10^{-5}$ mbar and pressure up to 40 bar. The experiments have been performed at 1.8 bar in helium with defined small amounts of impurities at 950 °C on thin walled tubes. A major problem was the axial and circumferential temperature distribution which was optimized to a deviation between two locations of better than 15 °C. The strain and

shear displacements have been measured with a newly developped extensometer of very high resolution. Uniaxial tension, torsion and biaxial experiments without and with 45° phase angle have been performed. The fatigue lives could consistently be described by the von Mises equivalent strain hypothesis without any modifications. The fatigue cracks mainly occured normal to the principal loading directions or in the case of 45° phase angle independently normal to the axial and shear strain directions. At 950 °C NiCr23Co12Mo practically shows no strain hardening which is believed to be the reason for the good fit of the fatigue results with the von Mises equivalent strain.

Acknowledgement

This work was performed with the support of the State of North Rhine Westfalia within the development of the Project Nuclear Process Heat, which is gratefully acknowledged. The authors would further like to thank Messr. Breuer and Burtscheid, who performed an important part of the configuration and installation work for the test facility.

References

[1] M.W. Brown, K.J. Miller
A theory for fatigue under multiaxial stress-strain conditions
Inst. Mech. Engrs 187, 1973, pp 745-755

[2] E. Krempl
The influence of state of stress on low-cycle fatigue of structural material
ASTM STP 549, 1974

[3] Y.S. Garud
Multiaxial fatigue: A survey of the state of the art
J. Test. Eval 9, 1981, pp 165-178

[4] H. Nickel, P. Ennis, F. Schubert, H. Schuster
Qualification of Metallic Materials for Application in Advanced High Temperature Gas-Cooled Reactors
Nucl. Techn. 58, 1982, pp 90 - 106

[5] M.S. Found, U.S. Fernando, K.J. Miller
Requirements of a New Multiaxial Fatigue Testing Facility in: Multiaxial Fatigue, ASTM STP 853
K.J. Miller, M.W. Brown Eds, 1985

[6] K.B.S. Rao, H.-P. Meurer, H. Schuster
Creep-Fatigue Interaction of Inconel 617 at 950 °C in Simulated Nuclear Reactor Helium
Mat. Science Engng A104, 1987, pp 37-51

[7] F. Richter
Thermophysikalische Eigenschaften des hochwarmfesten Werkstoffes NiCr22Co12Mo (Inconel 617)
Mat.-wiss. u. Werkstofftechnik 19, 1988, pp 55-61

[8] H.C. Wan, C.C. Yang
On the Influence of Strain-Path in Multiaxial Fatigue Failure
J. Eng. Materials and Technology 109, 1987, pp 107-113

Table I: Partial pressures of the impurities in the helium gas

| impurity: | $H_2$ | $CH_4$ | $H_2O$ | CO | $CO_2$ | $N_2$ |
|---|---|---|---|---|---|---|
| p (μbar) | 500 ± 50 | 20 ± 5 | 1.5 ± 1 | 15 ± 5 | 1.0 | 5 |

Table II: Chemical composition and room temperature properties

Chem. comp. (weight %)

| Heat | C | Cr | Mo | Al | Ti | Mn | Si | Co | S |
|---|---|---|---|---|---|---|---|---|---|
| 1 | 0.067 | 22.10 | 9.38 | 0.74 | 0.47 | 0.05 | 0.20 | 11.82 | 0.03 |
| 2 | 0.052 | 21.61 | 9.00 | 1.00 | 0.45 | 0.03 | 0.13 | 12.60 | 0.016 |
| specification | 0.04 | 20.0 | 8.00 | 0.60 | 0.2 | | | 10.00 | |
| | 0.08 | 23.0 | 10.00 | 1.30 | 0.6 | < 0.7 | 0.7 | 13.00 | < 0.015 |

Room temperature properties

| Heat | $R_{p0.2}$ / MPa | $R_m$ / MPa | $A_5$ / % |
|---|---|---|---|
| 1 | 362 - 382 | 775 - 824 | 61 |
| 2 | 357 - 391 | ~ 790 | 57 |

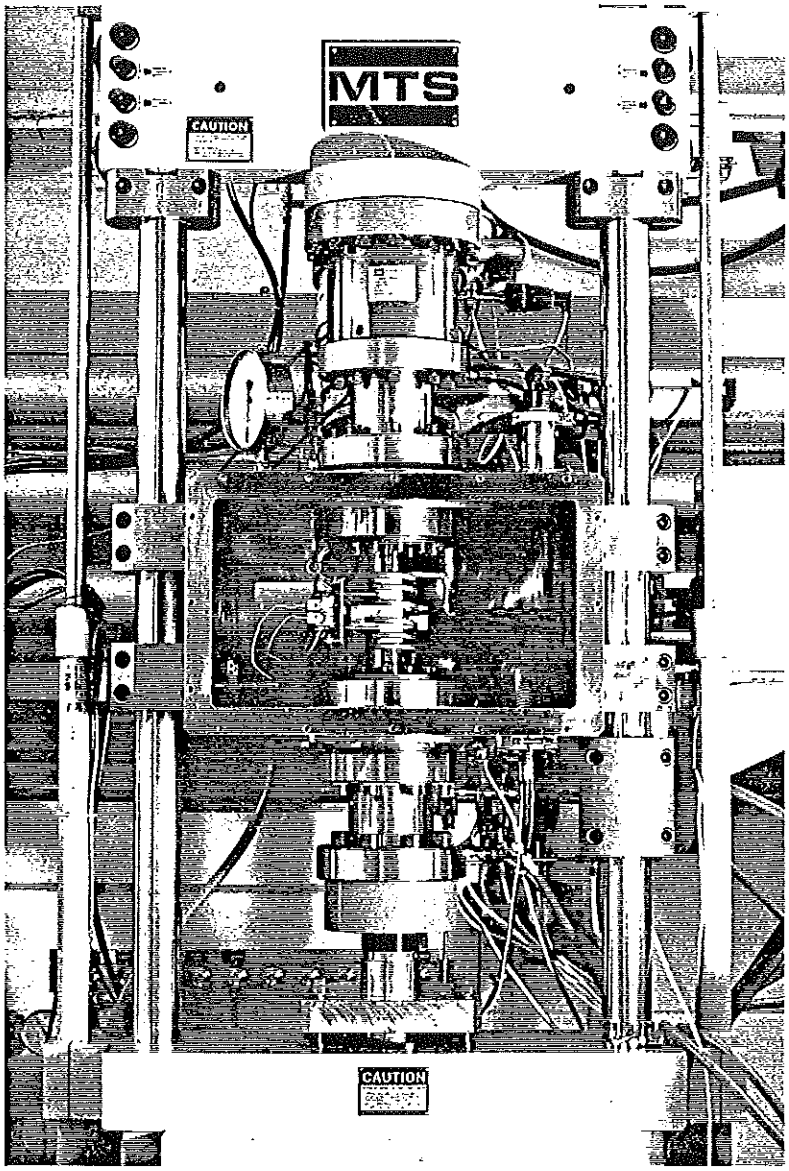


Fig. 1: Load frame with integrated pressure chamber

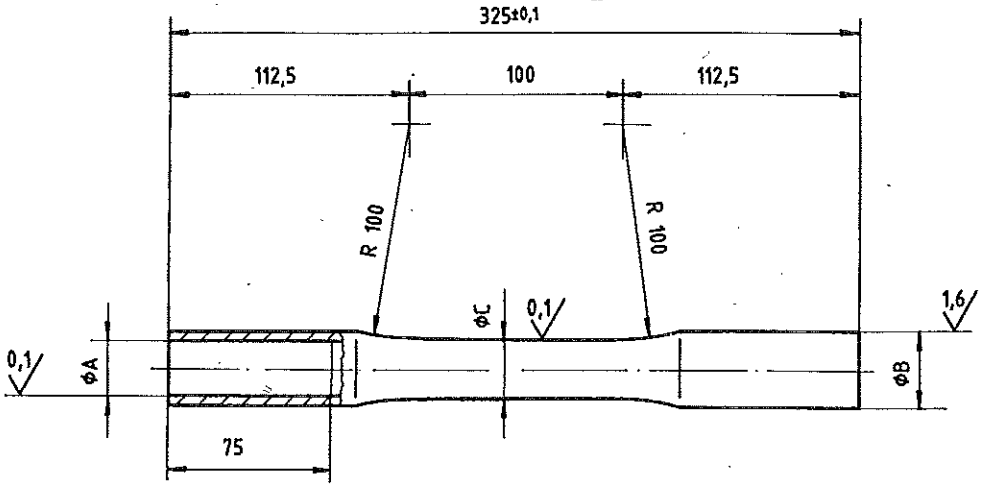


Fig. 2: Specimen geometry
Inner tube diameter A = 28 ± 0.025 mm
Outer tube diameter B = 33,2 ± 0.05 mm
Outer diameter gauge length C = 32 ± 0.01 mm

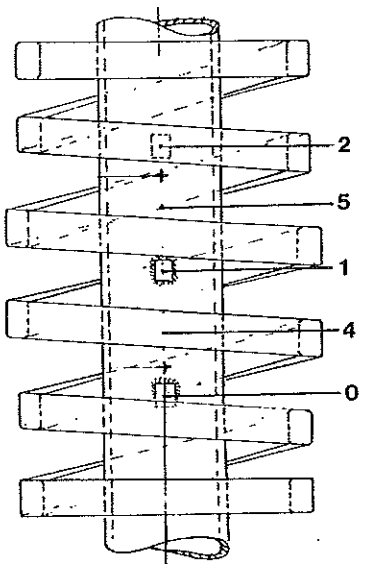


| Angle | Thermocouple position | | | | |
|---|---|---|---|---|---|
| | 0 | 4 | 1 | 5 | 2 |
| 0° | 950 | 950 | 950 | 954 | 952,5 |
| 45° | 952 | 953 | 952 | 957 | 956 |
| 90° | 956 | 954 | 955 | 958 | 958 |
| 135° | 958 | 950 | 955,5 | 958 | 956,5 |
| 180° | 958,5 | 945 | 954 | 954 | 953,5 |
| 225° | 956,5 | 944 | 951,5 | 951 | 950 |
| 270° | 953 | 945 | 950 | 949 | 949 |
| 315° | 951,5 | 945 | 949,5 | 949 | 949 |

Fig. 3: Geometry of the induction coil and temperature distribution on the specimen

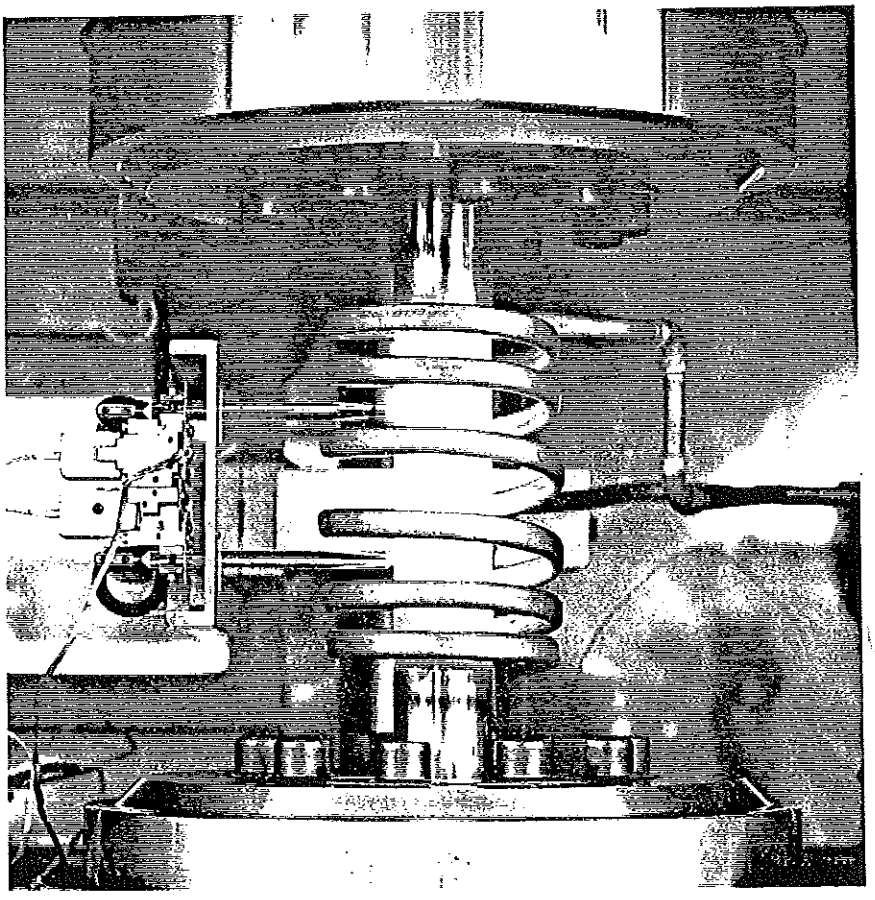

Fig. 4: Extensometer configuration

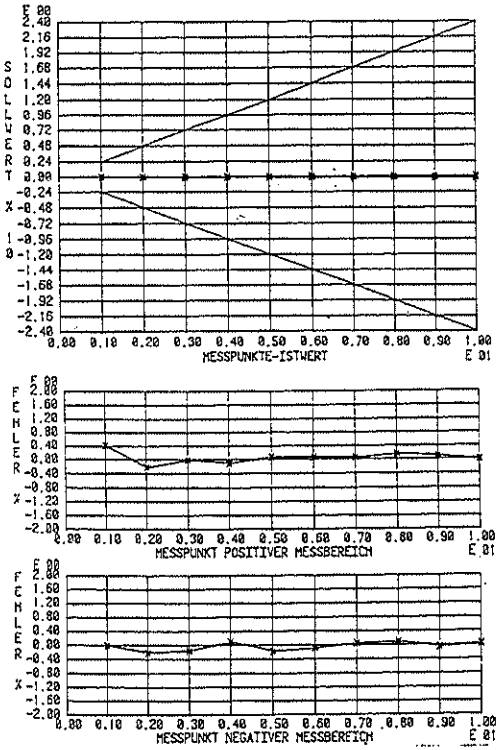


$\Delta\varepsilon_A = \pm\ 0.24\ \%,\ \Delta\phi = 0°$

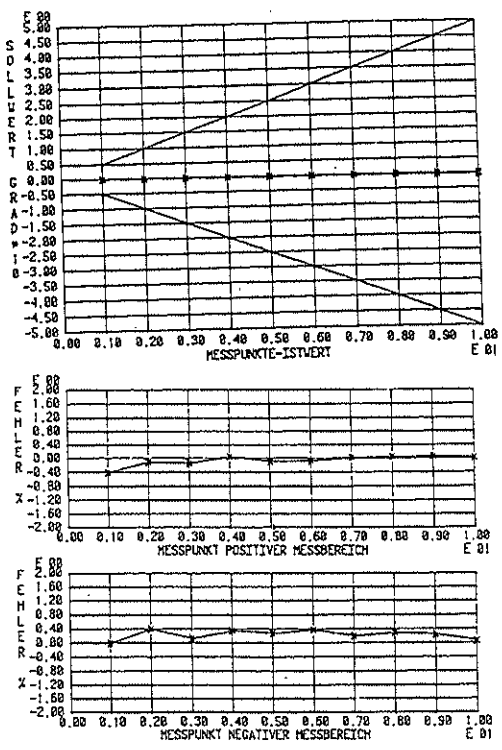


$\Delta\varepsilon_A = 0°,\ \Delta\phi = \pm\ 0.5°$

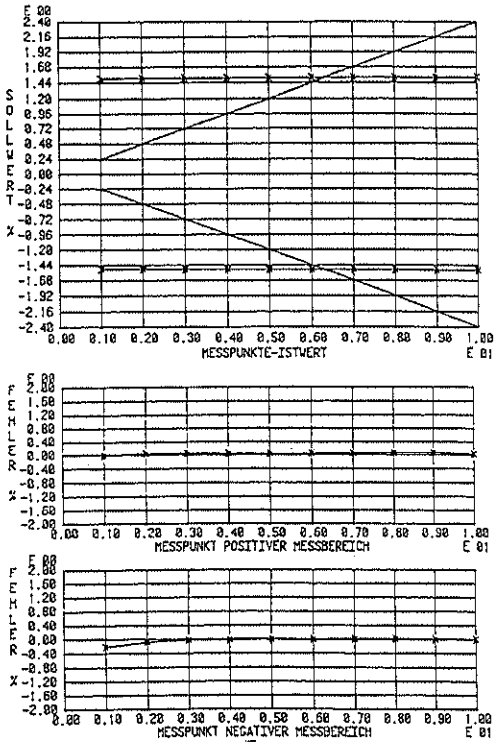


$\Delta\varepsilon_A = \pm\ 2.4\ \%,\ \phi = \pm\ 1.5°$

Fig. 5: Calibration diagrammes of the biaxial extensometer

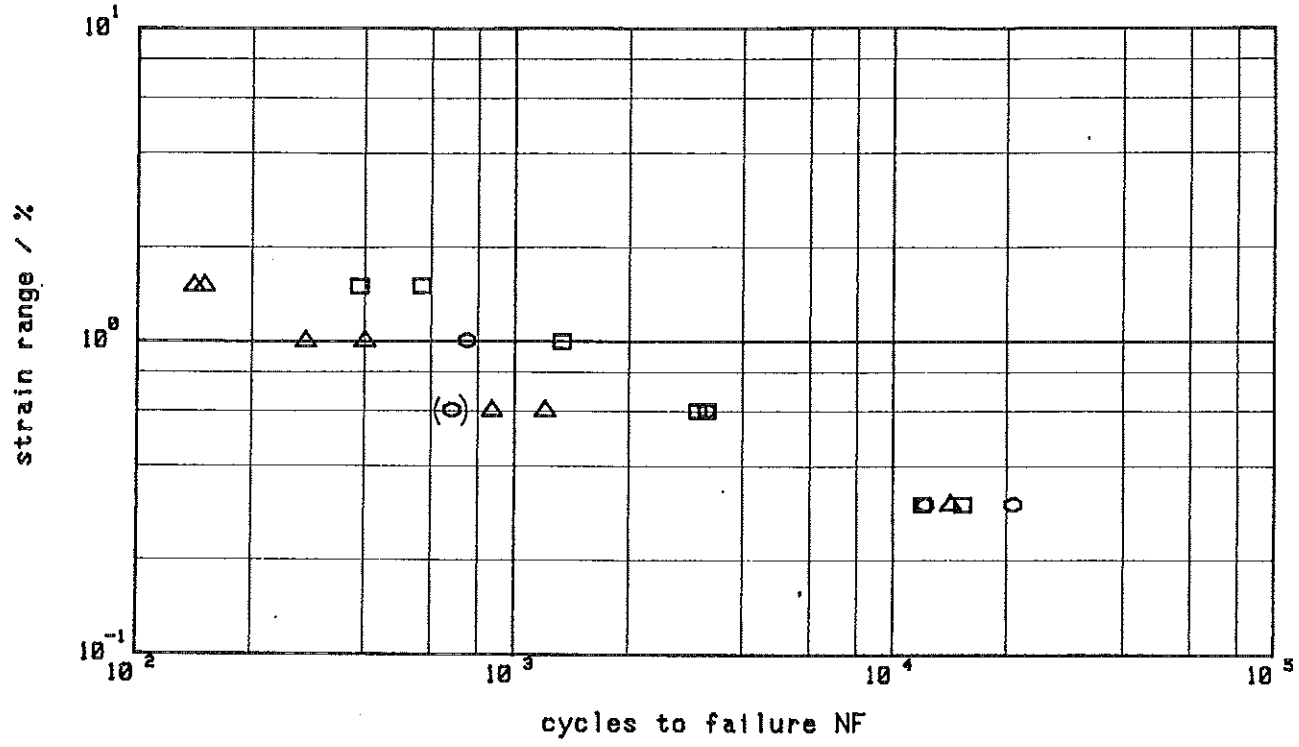


Fig. 6: Comparison of tubular and solid specimens at 950° C

○ thin walled tubes △ solid specimens ht.365 □ solid specimens ht.444

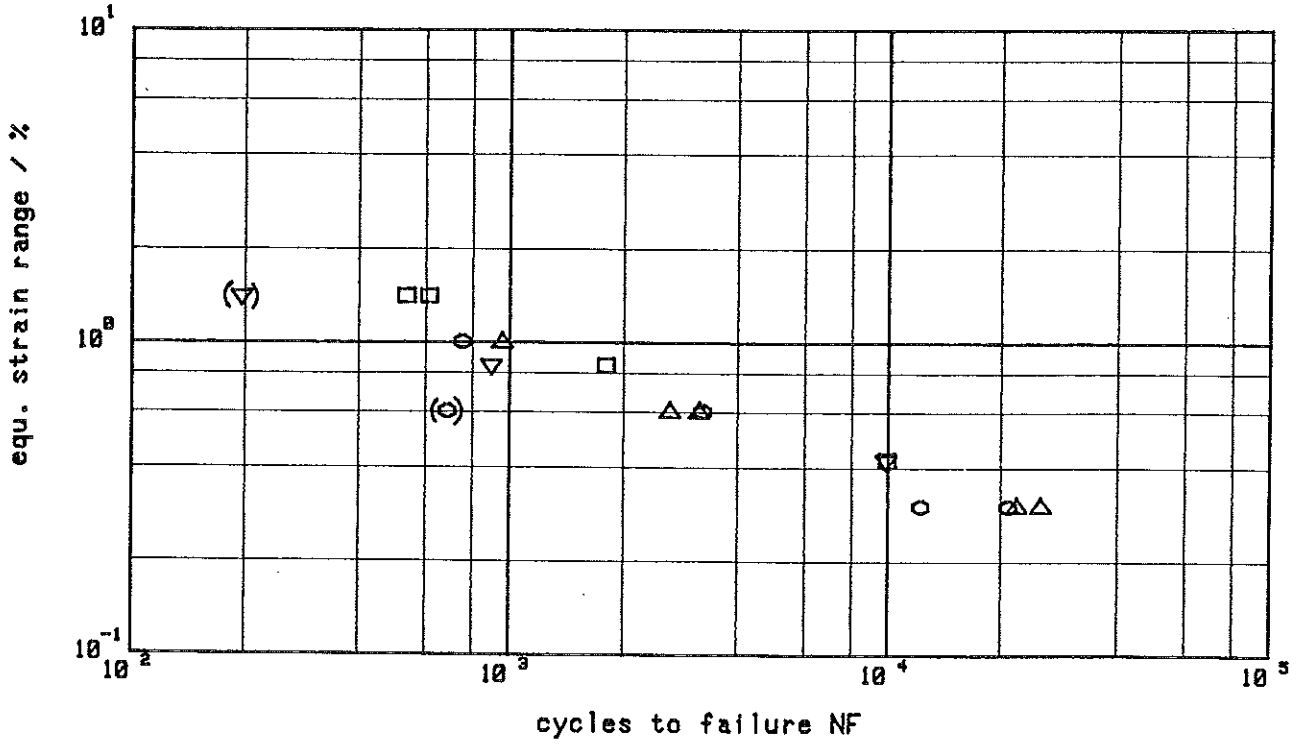


Fig. 7: Multiaxial fatigue behaviour of Inc.617 at 950° C

○ axial loading △ torsional loading □ ax. + tors. load. $\Phi = 0°$

▽ ax. + tors. loading $\Phi = 45°$

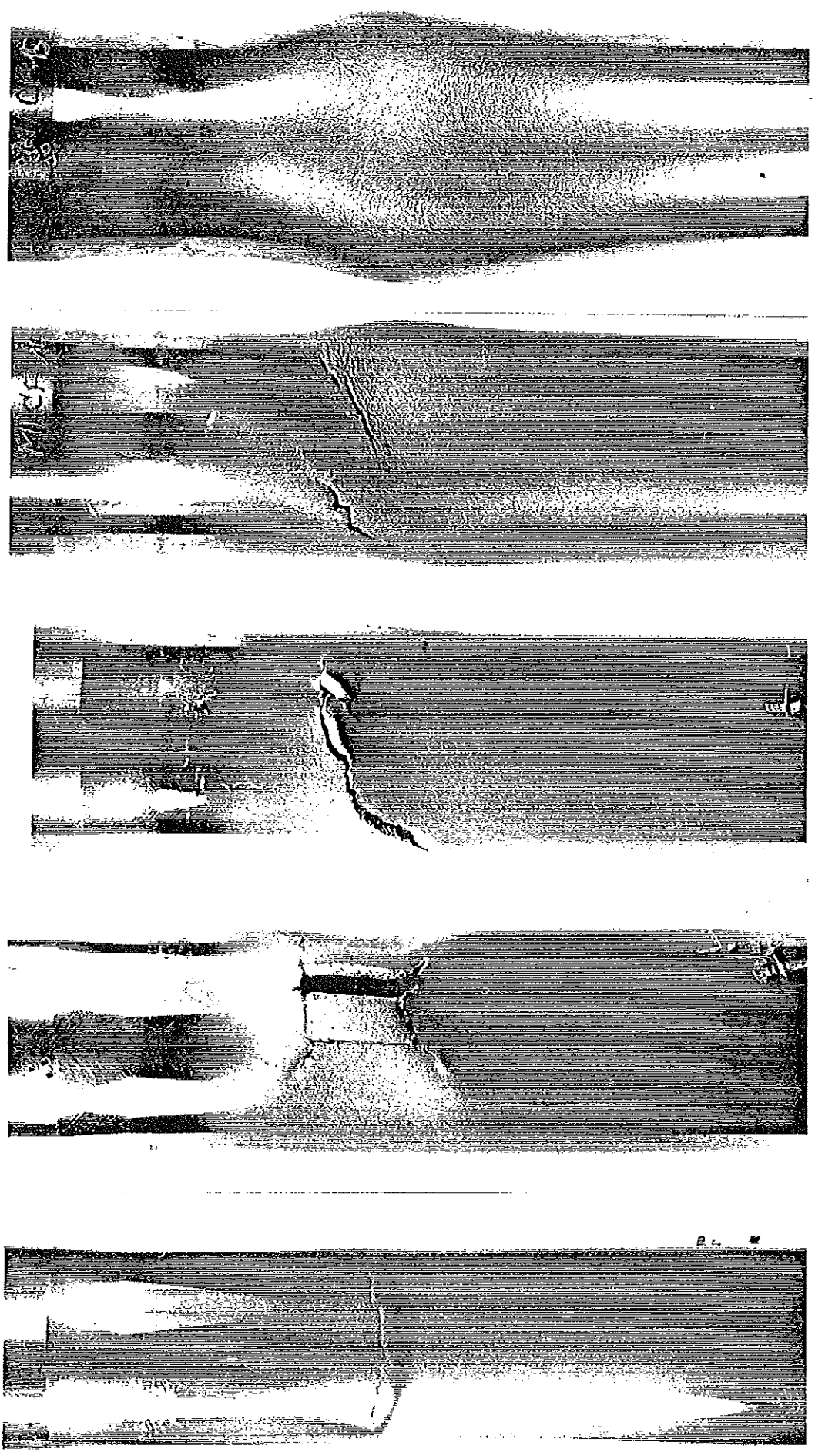


Fig. 8: Examples of failed specimens

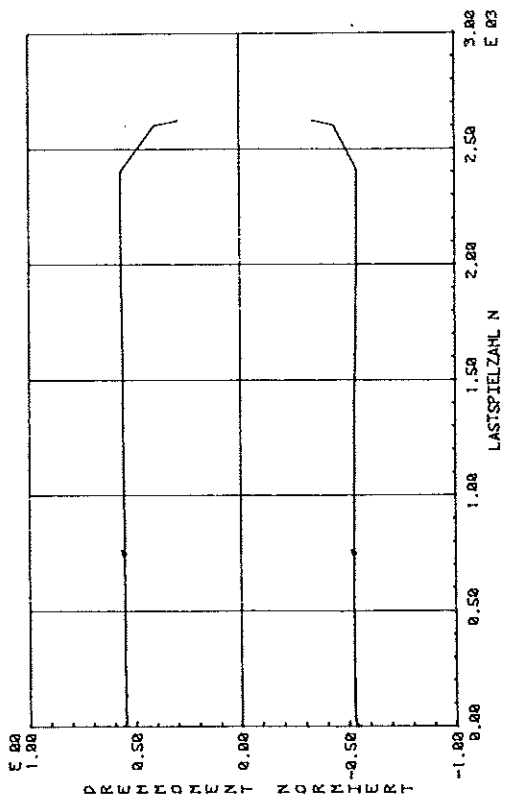


b) $\Delta\varepsilon_{MT} = 0.6$ %

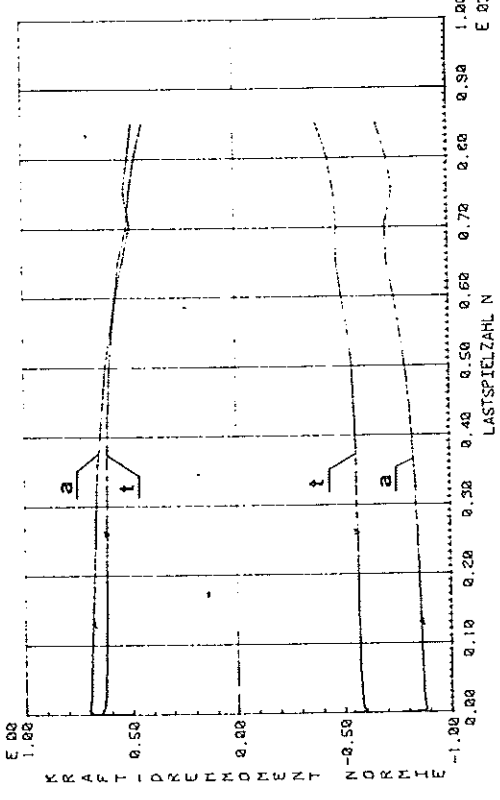


d) $\Delta\varepsilon_A = \Delta\varepsilon_{MT} = 0.6$ %, $\phi = 45°$

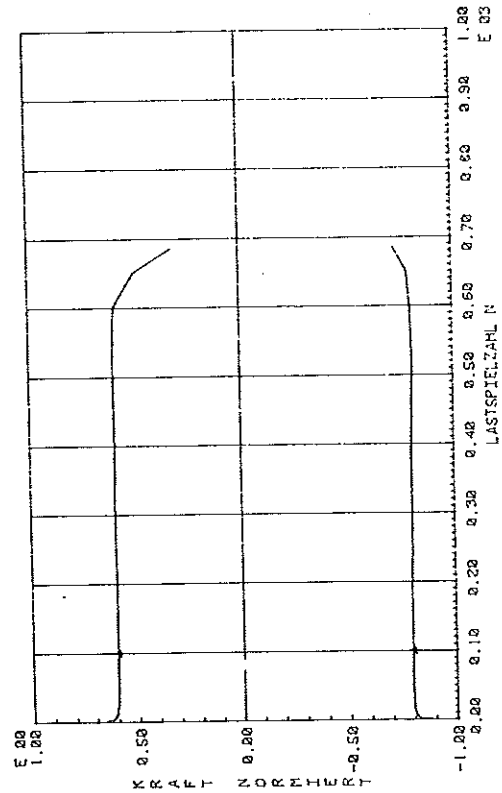


a) $\Delta\varepsilon_A = 0.6$ %

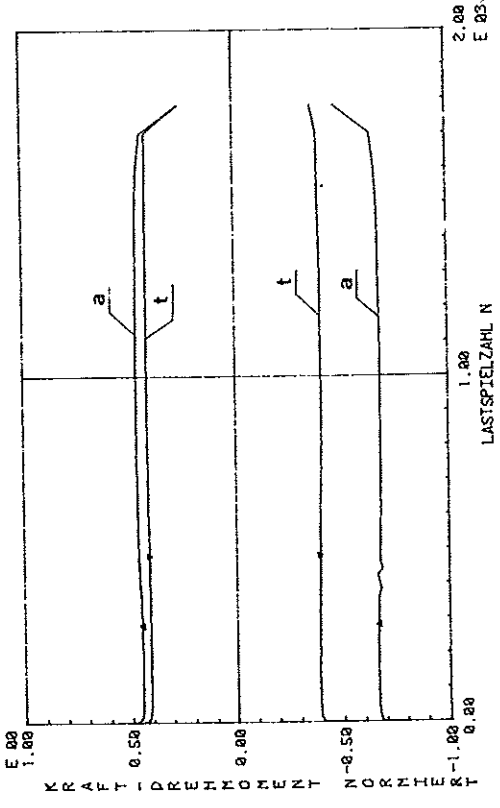


c) $\Delta\varepsilon_A = \Delta\varepsilon_{MT} = 0.6$ %, $\varnothing = 0°$

Fig. 9: Cyclic hardening behaviour at 0.6 % strain range ($c_a$ = 265 Nmm$^{-2}$, $c_t$ = 117.5 Nmm$^{-2}$)

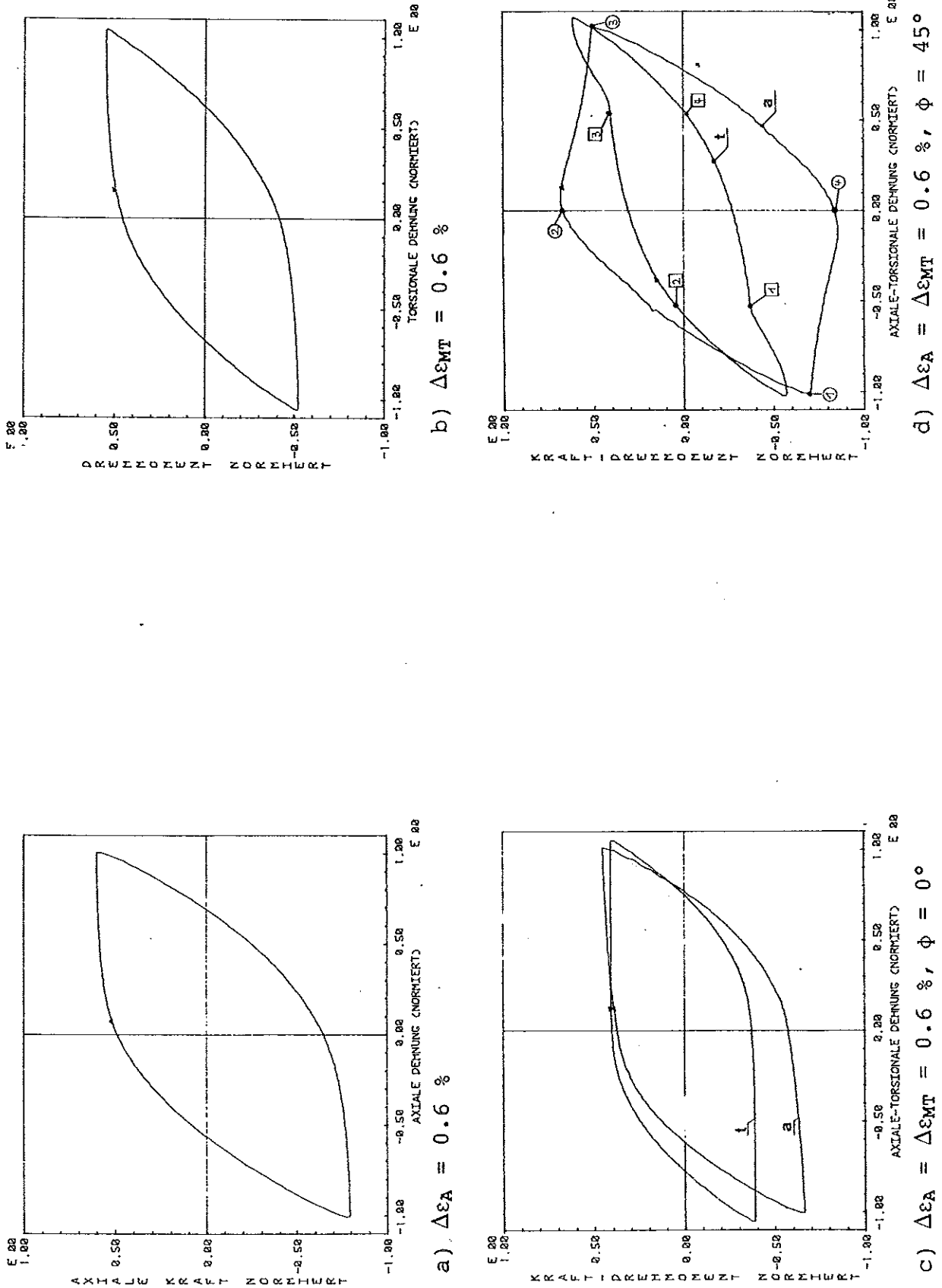


Fig. 10: Hysteresis loops at 0.6 % strain range ($c_a$ = 265 Nmm$^{-2}$, $c_t$ = 117.5 Nmm$^{-2}$)